GEOPHYSICS, VOL. 56, NO. 12 (DECEMBER 1991); P. 1940–1949, 14 FIGS., 1 TABLE.

Estimating grain-scale fluid effects on velocity dispersion in rocks

Gary Mavko* and Diane Jizba‡

ABSTRACT

The magnitude of the grain-scale local flow effect on velocity dispersion in saturated rocks is quantified, by estimating the high-frequency unrelaxed shear and bulk frame moduli, which are then combined with the Biot formulation to predict total dispersion. The method is relatively independent of assumptions about idealized pore geometries and unknown parameters such as pore aspect ratios. The local flow effect depends on the heterogeneity of pore stiffness, in particular the presence of compliant cracks and grain contacts; the pressure dependence of the dry rock properties is shown to contain the essential information about the distribution of pore stiffnesses needed to estimate the high-frequency saturated behavior. To first order, the unrelaxed wet frame compressibility at any given pressure is shown to be approximately the dry frame compressibility at very high pressure; second order corrections add the additional compressibility gained by replacing an amount of mineral equal to the compliant pore volume with fluid. The method predicts that the difference between relaxed and unrelaxed shear compliance is simply proportional to that in bulk. The results for total dispersion (local flow plus Biot) explain quite well the measured *P*- and *S*-wave dispersion for a variety of saturated rocks.

INTRODUCTION

It is well known that cracks and pores lower the elastic moduli of a rock relative to the moduli of its constituent minerals. Fluid saturation tends to restore some of the elastic stiffness, but in a way that often depends on frequency.

Gassmann (1951) derived a remarkably simple expression relating the saturated rock bulk modulus to the dry rock bulk modulus:

$$\frac{1}{K_{gs}} - \frac{1}{K_0} = \left(\frac{1}{K_f} - \frac{1}{K_0}\right) \times \phi \frac{1}{1 + \phi\left(\frac{1}{K_f} - \frac{1}{K_0}\right) \Big/ \left(\frac{1}{K_{\text{dry}}} - \frac{1}{K_0}\right)}, \tag{1}$$

where K_0, K_{dry}, and K_f are the bulk moduli of the mineral grains, the dry rock, and the pore fluid, respectively, and ϕ is the porosity. K_{gs} is the predicted saturated bulk modulus. Gassmann predicted no change for the shear modulus due to saturation:

$$\frac{1}{\mu_{gs}} = \frac{1}{\mu_{\text{dry}}}, \tag{2}$$

where μ_{gs} is the predicted saturated rock shear modulus, and μ_{dry} is the dry rock shear modulus.

Gassmann's result assumes statistical isotropy of the pore space but is otherwise completely independent of pore geometry. Unlike many other models, it does not assume idealized pore shapes (e.g., elliptical cracks); elastic interaction between pores is perfectly described. It is limited to frequencies that are low enough that inertial and scattering effects can be ignored and that the pore pressure induced by the externally applied stress is equilibrated over scales much larger than individual grains and pores. It also assumes that the moduli of the individual grains are identical.

Biot's (1956a, b) formulation for wave propagation in saturated solids includes coupling of fluid and solid stresses and the effects of contrasting inertial forces in the fluid and solid. But details of pore shape and local flow are neglected and lumped into parameters that relate only the averaged solid and fluid motions on a scale much larger than the pore size. The low-frequency limit of Biot's formulation for bulk and shear moduli is identical to Gassmann's. A modest dispersion in both bulk and shear is predicted at higher frequencies.

Manuscript received by the Editor January 29, 1990; revised manuscript received May 13, 1991.
*Department of Geophysics, Stanford University, Stanford, CA 94305-2215
‡Formerly Stanford University; presently SNEA(P), CSTJF, Avenue Larribau, 64018 Pau, France.

Measured seismic velocities at ultrasonic frequencies (Winkler, 1985, 1986) are often much faster than predicted by either the Gassmann or Biot formulations. Winkler found that the "non-Biot" dispersion tends to increase with frequency and fluid viscosity and to decrease with effective pressure. Both experiments (Murphy et al., 1984; Wang and Nur, 1988) and models (Mavko and Nur, 1979; O'Connell and Budiansky, 1974, 1977) suggest that the cause is related to the grain-scale microscopic flow field. When a section of rock is excited by a passing wave, heterogeneities, such as variations in pore shape, saturation, and orientation, are likely to produce pore pressure gradients and flow on the scale of individual pores. Unequilibrated pressures make the rock stiffer in both bulk and shear than do equilibrated pressures. Because the average of the local flow over many pores is zero, this mechanism is ignored in the original Biot (1956a, b) model. Biot (1962a, b) subsequently suggested the idea of local flow, but it wasn't pursued by other authors until much later.

This paper quantifies the effects of grain-scale local flow on both bulk and shear dispersion, by estimating the high-frequency, unrelaxed bulk and shear moduli. It differs from previous discussions (Mavko and Nur, 1979; O'Connell and Budiansky, 1974, 1977; Coyner and Cheng, 1985; Murphy et al., 1984) in that it is relatively independent of specific crack geometries like ellipses, aspect ratios, etc. It is more like the results of Gassmann (1951) in that the unrelaxed saturated moduli are estimated directly from K_{dry}, K_0, K_f, and ϕ with the additional information $\phi(p)$ and $K_{dry}(p)$. These two dry pressure dependent quantities carry the necessary information about the distribution of pore stiffness.

The results, when combined with Biot's (1956a, b), explain fairly well the measured total compressional- and shear-wave dispersion for a variety of saturated rocks.

Local flow in the Biot formulation

We incorporate the effects of unrelaxed local pressures in the way suggested by Biot (1962a, b), Stoll and Bryan (1970), and Keller (1989). The elastic dry mineral frame in Biot's earlier (1956a, b) formulation is replaced with a viscoelastic frame. We explicitly treat only the high- and low-frequency limits of the frame behavior that can be accurately treated as two separate elastic states. We do not explore the frequency dependence in between, because it depends more explicitly on the details of pore geometry (Mavko and Nur, 1979; O'Connell and Budiansky, 1977; Murphy et al., 1984). Our goal is to estimate the magnitude of dispersion with the fewest assumptions about the unknown pore geometry. We will use the term "dispersion" to refer to the difference between the low-frequency Gassmann estimate of velocity and the observed or predicted high-frequency velocity as done by other authors (Winkler, 1985, 1986; Wang and Nur, 1988).

Consider a saturated rock sample with the pore space vented to zero pore pressure. When a load is applied to the rock at very low frequencies, pore fluid can easily flow in and out of every pore, so that the drained frame moduli are essentially the same as dry rock moduli. However, at higher frequencies, viscous effects cause the thinnest pores to be isolated with respect to flow. Unrelaxed pore pressures are induced in these pores, so that the frame is now only *partially drained* and is stiffer than at low frequencies. We will refer to this as the *unrelaxed frame*.

We proceed now to derive an expression for the unrelaxed frame bulk and shear moduli in terms of the measurable pressure dependence of dry rock moduli. We show that the unrelaxed frame compressibility at any pressure is approximately the very high pressure dry rock compressibility plus a second order correction proportional to the porosity change that occurs with increasing confining pressure. We also show that the stiffening in shear is simply proportional to that in bulk. These frame moduli are then used in the more conventional Biot (1956a, b) formulation to predict total dispersion.

DERIVATION OF UNRELAXED FRAME BULK MODULUS

Consider the rock to be a linear, isotropic, homogeneous, elastic, mineral material penetrated with pore space of arbitrary shape and complexity. When the rock is saturated and instantaneously loaded in compression, pressure is induced in the pore fluid. Stiff portions of the pore space tend to shelter the fluid and therefore have relatively low induced pore pressure; compliant portions of the pore space tend to transfer more of the stress to the fluid and therefore have a relatively high induced pore pressure. At low frequencies one expects these pressures to equilibrate, but at very high frequencies at least some of the pore pressure gradients should persist.

We can estimate quantitatively the effect of this uneven pore pressure distribution on the instantaneous bulk modulus using the Betti-Rayleigh reciprocity theorem (Walsh, 1965; Jaeger and Cook, 1969). Consider the two sets of tractions applied to a rock with total volume V, as shown in Figure 1. The system on the left is loaded by an externally applied, uniform, hydrostatic stress $\Delta\sigma$. Internally applied tractions $\Delta P(x, y, z)$, (which are equal to the as yet unknown spatially variable induced pore pressures) are applied to the unrelaxed fraction of the pore space. Zero internal tractions are assumed on the drained fraction of the pore space. The system on the right has the same uniform stress $\Delta\sigma$ applied to both external and internal surfaces. In this case the rock behaves like a solid block without pores. Applying the reciprocity theorem, we can write:

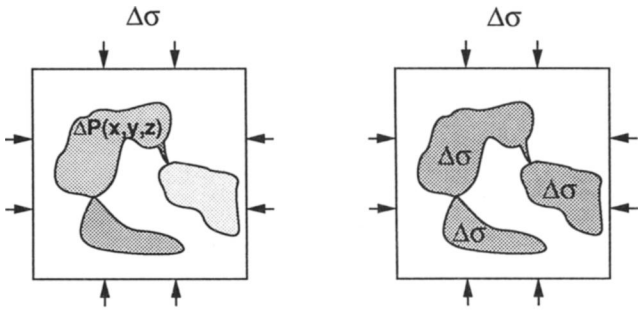

FIG. 1. Two sets of tractions applied to the same rock sample. The sample on the left behaves as an unrelaxed, saturated rock. The sample on the right behaves as a rock without pores.

$$\Delta\sigma \frac{\Delta\sigma}{K_{uf}} V - \sum_{i_{\text{unrelaxed}}} \Delta\sigma \Delta v_{pi} - \Delta\sigma \Delta v_{p\text{-drained}}$$

$$= \Delta\sigma \frac{\Delta\sigma}{K_0} V - \sum_{i_{\text{unrelaxed}}} \Delta P_i \frac{\Delta\sigma}{K_0} v_{pi}, \qquad (3)$$

where K_{uf} is the unrelaxed frame bulk modulus that we seek. The effect of viscous shear tractions on the pore walls does not appear, because the "solid block" displacements of the system on the right are exactly normal to the pore walls, giving a zero contribution to the work done. The summations result from separating the integrals of work done on the pore walls into the sum of integrals over subsets of the pore space. This separation is simply a mathematical operation. It does not reduce the generality of the result, and it retains full elastic pore interaction. The subsets can be chosen in any convenient way. In this discussion, we partition the pore space into the drained fraction plus subsets of the unrelaxed fraction having approximately equal induced pore pressure, ΔP_i. Correspondingly, v_{pi} is the volume of that subset of pore space and Δv_{pi} is the stress-induced change of pore volume; $v_{p\text{-drained}}$ is the drained pore volume. The summation now has the interpretation of summing over all unrelaxed pore pressures. Dividing each term in equation (3) by $(\Delta\sigma)^2 V$ and taking the limit as $\Delta\sigma \to 0$ gives

$$\frac{1}{K_{uf}} - \frac{1}{K_0} = \left(\frac{d\phi}{d\sigma}\right)_{\text{drained}} + \sum_{\substack{\text{low } P \\ \text{unrelaxed}}}^{\text{high } P} \left(\frac{d\phi_i}{d\sigma}\right) - \sum_{\substack{\text{low } P \\ \text{unrelaxed}}}^{\text{high } P} \frac{\phi_i}{K_0} \frac{dP_i}{d\sigma}, \qquad (4)$$

where $\phi_i = v_{pi}/V$ is the porosity of the ith subset of pore space, and $(d\phi_i/d\sigma)$ is its saturated compressibility. Finally, combining equation (4) with the definition of the fluid bulk modulus, $\Delta P_i = K_f \Delta\phi_i/\phi_i$ gives:

$$\frac{1}{K_{uf}} - \frac{1}{K_0} = \left(\frac{d\phi}{d\sigma}\right)_{\text{drained}} + \left(\frac{1}{K_f} - \frac{1}{K_0}\right) \times \sum_{\substack{\text{low } P \\ \text{unrelaxed}}}^{\text{high } P} \phi_i \frac{dP_i}{d\sigma}. \qquad (5)$$

To this point, no specific assumptions have been made about the shape of the pore space, except that the moduli of the mineral grains are the same, as assumed by Gassmann's derivation. In fact, if $dP_i/d\sigma$ is uniform throughout the entire pore space, then equation (5) leads to Gassmann's relation, equation (1), with $K_{uf} \to K_{gs}$.

We now estimate the stress-induced pore pressure in the ith subset of unrelaxed pore space. The change in volume Δv_{pi} of the ith subset can be decomposed as illustrated in Figure 2. By linear superposition, the displacements in the saturated rock can be expressed as the sum of displacements in a dry rock with externally applied stress $(\Delta\sigma - \Delta P_i)$ plus the displacements of the same rock with stress ΔP_i applied to the external boundary as well as throughout the ith fraction of pore space. All other pores are subject to their respective pore pressures ΔP_j, ΔP_k, etc., or zero, if drained. The change in the ith saturated pore volume can then be written as

$$(\Delta v_{pi}) \approx \left(\frac{dv_{pi}}{d\sigma}\right)_{\text{dry}} (\Delta\sigma - \Delta P_i) + \frac{\Delta P_i}{K_0^*} v_{pi}. \qquad (6)$$

The first term on the right side of equation (6) is proportional to the exact dry-rock pore volume compressibility of the ith subset, including all interaction with other pores. The second term on the right is approximately the volume change that would occur if the rock were solid with no pore space. It would be exactly $\Delta P_i v_{pi}/K_0$ if all pore pressures were equal to P_i. It is more appropriately estimated with some effective modulus $K_0^* \approx K_0$. However, we believe that this uncertainty is of little consequence, since the contribution of this term is small, as shown below.

Equating the volume change in equation (6) with the volume change of the compressible fluid, $(\Delta v_{pi}) = \Delta P_i v_{pi}/K_f$ and taking the limit $\Delta\sigma \to 0$ gives

$$\frac{dP_i}{d\sigma} \approx \frac{1}{1 + \left(\frac{1}{K_f} - \frac{1}{K_0^*}\right) \phi_i/(d\phi_i/d\sigma)_{\text{dry}}}. \qquad (7)$$

We see that if $K_f \ll K_0 \approx K_0^*$, as is usually the case, then the error in substituting K_0 for K_0^* is negligible. Finally, combining equations (5) and (7) gives

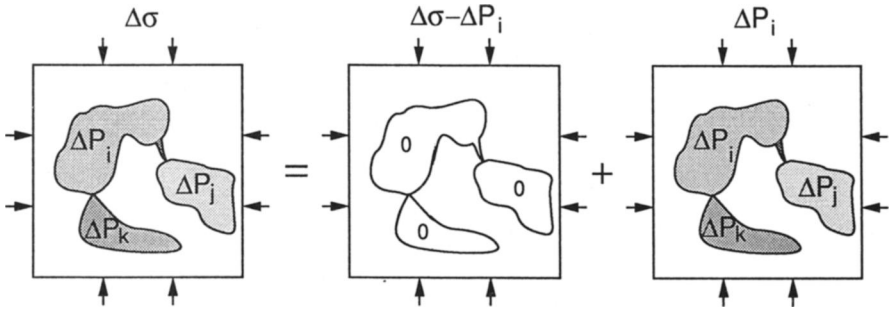

FIG. 2. Decomposition of stresses applied to the saturated rock, in order to estimate the pore pressure induced in the ith subset of the pore space.

$$\frac{1}{K_{uf}} - \frac{1}{K_0} \approx \left(\frac{d\phi}{d\sigma}\right)_{\text{drained}} + \left(\frac{1}{K_f} - \frac{1}{K_0}\right) \times \sum_{\substack{\text{low } P \\ \text{unrelaxed}}}^{\text{high } P} \frac{\phi_i}{1 + \left(\frac{1}{K_f} - \frac{1}{K_0}\right)\phi_i/(d\phi_i/d\sigma)_{\text{dry}}}. \quad (8)$$

This is the desired expression for unrelaxed frame modulus in terms of dry rock properties.

We now assume that the drained term in equation (8) can be estimated from the dry rock compressibility at high confining pressure. This assumes that the unrelaxed pore space is the softest portion of the pore space, such as thin cracks and grain contacts, and that at sufficiently high confining pressure, most of this soft porosity is compressed closed, or at least substantially reduced in volume. This is consistent with the observation that non-Biot dispersion tends to decrease at high pressure. Substituting $(d\phi/d\sigma)_{\text{drained}} = (1/K_{\text{dry}} - 1/K_0)_{\text{high}\sigma}$ into equation (8) and subtracting $1/K_0$ from both sides gives

$$\frac{1}{K_{uf}(\sigma)} \approx \left(\frac{1}{K_{\text{dry}}}\right)_{\text{high }\sigma} + \left(\frac{1}{K_f} - \frac{1}{K_0}\right) \times \sum_{\text{soft porosity}} \frac{\phi_i}{1 + \left(\frac{1}{K_f} - \frac{1}{K_0}\right)\phi_i/(d\phi_i/d\sigma)_{\text{dry}}}. \quad (9)$$

The denominator in the summation is close to unity for soft porosity, so that it can be expanded in numerator form, giving

$$\frac{1}{K_{uf}(\sigma)} \approx \left(\frac{1}{K_{\text{dry}}}\right)_{\text{high }\sigma} + \left(\frac{1}{K_f} - \frac{1}{K_0}\right)\phi_{\text{soft}}(\sigma) - \left(\frac{1}{K_f} - \frac{1}{K_0}\right)^2 \sum_{\text{soft porosity}} \frac{\phi_i^2}{\frac{d\phi_i}{d\sigma}} + \ldots. \quad (10)$$

Finally, we end up with the very simple and intuitive result that to first order the unrelaxed frame compressibility is approximately the dry frame compressibility at high confining pressure; to second order we add the extra compressibility gained by replacing an amount of mineral equal to the soft pore volume with fluid. These first two terms represent the effect of a bimodal distribution of stiff plus soft porosity, and for many cases only the first is required. The higher terms correct for intermediate pore stiffness, and can often by ignored.

DERIVATION OF UNRELAXED FRAME SHEAR MODULUS

Consider the same rock model. When the rock is saturated with some pore fluid and instantaneously loaded in *shear*, pore pressure changes are again induced. Stiff equidimensional pores have low induced pore pressure, because compressive pore deformation in one direction approximately cancels extentional pore deformation in a perpendicular direction. Compliant portions of the pore space are not equidimensional, so that these deformations do not cancel.

We estimate the effect of the induced pore pressures on the unrelaxed frame shear modulus again using the reciprocity theorem. Consider the two sets of tractions applied to a rock as shown in Figure 3. The system on the left is loaded by an externally applied pure shear stress field with magnitude $\Delta\tau$. Internally applied tractions $\Delta P(x, y, z)$ (which are the as yet unknown, spatially variable, induced pore pressures) are applied to the unrelaxed pores, and zero tractions are applied to the drained pores. The system on the right has the externally applied tractions of magnitude $\Delta\tau$ applied to the external surfaces and zero tractions applied internally. Applying the reciprocity theorem, we can write:

$$\Delta\tau \frac{\Delta\tau}{\mu_{uf}} V = \Delta\tau \frac{\Delta\tau}{\mu_{\text{dry}}} V + \int\int_{\text{unrelaxed}} \Delta P \Delta u_n \, dA, \quad (11)$$

where μ_{uf} is the unrelaxed frame modulus that we seek, μ_{dry} is the dry rock shear modulus, and Δu_n is the component of dry rock pore wall displacement normal to the pore faces. The integral is over the pore faces. If we again divide the pore space into small subsets and take the limit $\Delta\tau \to 0$, the equation (11) can be written as:

$$\frac{1}{\mu_{\text{dry}}} - \frac{1}{\mu_{uf}} = \sum_{\text{low } P}^{\text{high } P} \frac{dP_i}{d\tau}\left(\frac{d\phi_i}{d\tau}\right)_{\text{dry}}, \quad (12)$$

where the summation is only over soft unrelaxed subsets of the pore space, each having induced pore pressure ΔP_i and porosity ϕ_i.

We now estimate the shear stress-induced pore pressure in the ith subset of pore space. Using superposition, the change in volume Δv_{pi} of the ith subset can be decomposed, as illustrated in Figure 4,

$$(\Delta v_{pi})_{\text{sat}} = \left(\frac{dv_{pi}}{d\tau}\right)_{\text{dry}} \Delta\tau - \left(\frac{dv_{pi}}{d\sigma}\right)_{\text{dry}} \Delta P_i + \frac{\Delta P_i}{K_0} v_{pi}. \quad (13)$$

The first term on the right side of equation (13) is proportional to the exact dry-rock shear-induced pore volume compressibility of the ith subset, including all interaction with other pores; the second term is the exact dry rock compression-induced pore volume compressibility of the ith pore; the last term is approximately the volume change that would occur if the rock were solid with no pore space. As

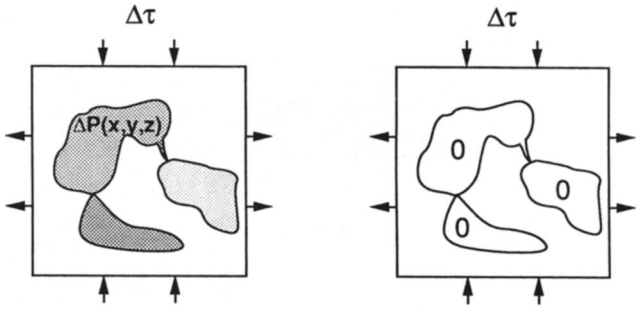

FIG. 3. Two sets of tractions applied to the same rock sample. The rock on the left deforms with the unrelaxed frame shear modulus. The rock on the right deforms with the dry shear modulus.

with the bulk modulus problem, it would be exactly $\Delta P_i v_{pi}/K_0$ if all pore pressures were equal to P_i. Equating equation (13) with the volume change of the fluid, $(\Delta v_{pi})_{\text{sat}} = \Delta P_i v_{pi}/K_f$ and taking the limit $\Delta\tau \to 0$ gives:

$$\frac{dP_i}{d\tau} \approx \frac{\left(\frac{d\phi_i}{d\tau}\right)_{\text{dry}}}{\left(\frac{d\sigma_i}{d\sigma}\right)_{\text{dry}} + \left(\frac{1}{K_f} - \frac{1}{K_0}\right)\phi_i}. \tag{14}$$

Finally, combining equations (12) and (14) gives

$$\frac{1}{\mu_{\text{dry}}} - \frac{1}{\mu_{uf}} \approx \sum_{\text{low } P}^{\text{high } P} \frac{\left(\frac{d\phi_i}{d\tau}\right)^2_{\text{dry}}}{\left(\frac{d\phi_i}{d\sigma}\right)_{\text{dry}} + \left(\frac{1}{K_f} - \frac{1}{K_0}\right)\phi_i}. \tag{15}$$

This is the desired expression for shear dispersion in terms of dry rock properties.

To estimate the shear induced dry compressibility $(d\phi_i/d\tau)$, we assume, as discussed above, that in an applied shear field significant pore pressure can only be induced in compliant, nonequidimensional pieces of pore space. We assume, therefore, that for each compliant pore there is some direction along which the resolved increment of normal stress $\Delta\sigma_n$ will cause the maximum compression of the pore. For example, this direction would be the normal to the faces of a crack or grain contact. We further assume that if the pore is sufficiently compliant to have a significant induced pore pressure, then components of stress perpendicular to the normal direction can be ignored. Then we approximate the shear induced compressibility of the ith pore as

$$\frac{d\phi_i}{d\tau} \approx \frac{d\phi_i}{d\sigma}\frac{d\sigma_n}{d\tau}, \tag{16}$$

where $d\phi_i/d\tau$ is the shear stress-induced dry rock pore compressibility, $d\phi_i/d\sigma$ is the compression-induced dry pore compressibility, and $d\sigma_n/d\tau$ is the ratio of normal stress in a particular direction to the magnitude of the applied shear stress.

Using the spherical coordinates shown in Figure 5, the normal stress $\Delta\sigma_n$ is

$$\Delta\sigma_n = \Delta\tau \sin^2\gamma(\cos^2\theta - \sin^2\theta)$$

or

$$\frac{d\sigma_n}{d\tau} = \sin^2\gamma(\cos^2\theta - \sin^2\theta). \tag{17}$$

Equation (15) can now be rewritten as

$$\frac{1}{\mu_{\text{dry}}} - \frac{1}{\mu_{uf}} \approx \sum_{\text{low } P}^{\text{high } P} \frac{1}{4\pi}\sum_{\theta}\sum_{\gamma} \frac{\left(\frac{d\phi_i}{d\tau}\right)^2_{\text{dry}}}{\left(\frac{d\phi_i}{d\sigma}\right)_{\text{dry}} + \left(\frac{1}{K_f} - \frac{1}{K_0}\right)\phi_i}, \tag{18}$$

where the summation over all unrelaxed pores is separated into summations over all normal directions and all pore stiffnesses. Substituting equations (16) and (17) into equation (18) gives

$$\frac{1}{\mu_{\text{dry}}} - \frac{1}{\mu_{uf}} \approx \frac{1}{4\pi} \sum_{\text{low } P}^{\text{high } P} \frac{\left(\frac{d\phi_i}{d\sigma}\right)^2_{\text{dry}}}{\left(\frac{d\phi_i}{d\sigma}\right)_{\text{dry}} + \left(\frac{1}{K_f} - \frac{1}{K_0}\right)\phi_i} \times \sum_{\theta}\sum_{\gamma} \sin^4\gamma(\cos^2\theta - \sin^2\theta)^2. \tag{19}$$

If we assume a uniform distribution of pore orientations and approximate the angular summation in (19) by an integral then equation (19) becomes

$$\frac{1}{\mu_{\text{dry}}} - \frac{1}{\mu_{uf}} \approx \frac{4}{15} \sum_{\text{low } P}^{\text{high } P} \frac{\left(\frac{d\phi_i}{d\sigma}\right)_{\text{dry}}}{1 + \left(\frac{1}{K_f} - \frac{1}{K_0}\right)\phi_i \Big/ \left(\frac{d\phi_i}{d\sigma}\right)_{\text{dry}}}. \tag{20}$$

(A non-uniform distribution gives an anisotropic behavior which will be treated in another paper.) As with the derivation for bulk modulus, the denominator can be expanded in numerator form to give:

$$\frac{1}{\mu_{\text{dry}}} - \frac{1}{\mu_{uf}} \approx \frac{4}{15}\left(\frac{d\phi_{\text{soft}}}{d\sigma}\right)_{\text{dry}} - \frac{4}{15}\left(\frac{1}{K_f} - \frac{1}{K_0}\right)\phi_{\text{soft}} + \cdots, \tag{21}$$

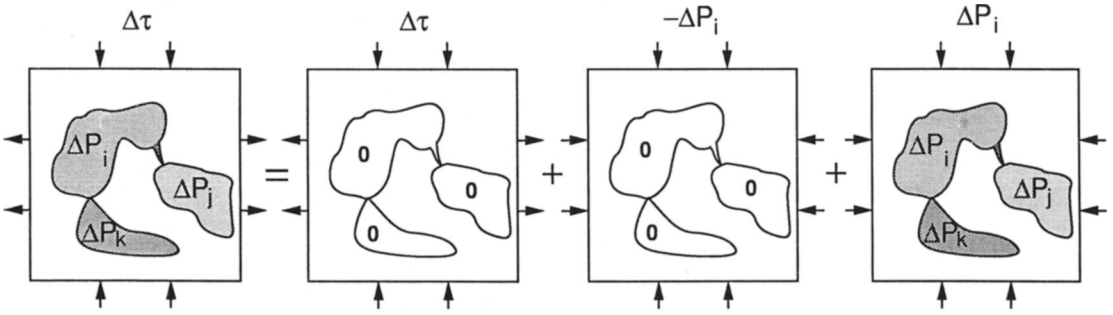

FIG. 4. Decomposition of stresses applied to the saturated rock, in order to estimate the pore pressure induced in the ith subset of the pore space.

which, can be written using equation (10) as:

$$\frac{1}{\mu_{dry}} - \frac{1}{\mu_{uf}} \approx \frac{4}{15}\left(\frac{1}{K_{dry}(\sigma)} - \frac{1}{K_{uf}(\sigma)}\right). \quad (22)$$

Equation (22) shows that the shear frame dispersion is proportional to the bulk frame dispersion. The indicated coupling of shear dispersion to bulk dispersion has important significance. A simple interpretation is that thin, crack-like, soft porosity dominates local flow dispersion; the difference between shear and bulk behavior results simply from the geometrically different orientation of compressive stresses that the cracks are subject to.

COMPARISON WITH EXPERIMENTAL DATA

In this section we use our model to predict high frequency saturated velocities in four rocks which span a range of porosity from .8 to 16 percent. We compare our predictions with the observed high frequency laboratory data, with high-frequency predictions of Biot (1956a, b), and with low frequency predictions of Gassmann (1951). Input parameters used in the Biot and Gassmann models are the dry bulk and shear moduli, K_{dry} and μ_{dry}, respectively (computed from the dry P- and S-wave velocity data), the porosity, grain density, and mineral bulk modulus K_0. The properties listed in Table 1 are all laboratory measured values, except for the mineral bulk moduli for Fontainebleau and the tight gas sandstone. For these two rocks we use a value of 38 GPa for quartz (Carmicheal, 1981). Variation of the mineral bulk modulus within a reasonable range of ±5 percent has a negligible impact on the computed P- and S-wave velocities for these two rocks. In addition, a tortuosity factor set equal to 2.0 is used in the Biot model predictions for all of the rocks. We find that variation of tortuosity within a typical range of one to three has a negligible impact on calculated velocities.

To calculate high-frequency saturated unrelaxed velocities (UV) we first computed the unrelaxed frame bulk and shear moduli, K_{uf} and μ_{uf}, from equations (10) and (22). We then used these in Biot's theory to estimate the high-frequency saturated unrelaxed velocities. We computed the model predictions at each stress where dry velocities were measured. We estimated the volume of soft porosity at any pressure as the difference between the total porosity and the extrapolation of the high-pressure porosity versus pressure trend.

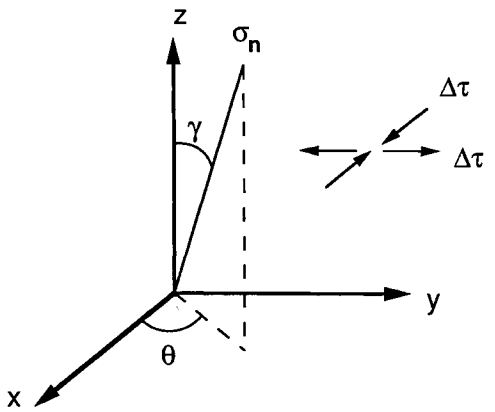

FIG. 5. Coordinate system of the normal direction relative to the applied shear field.

Westerly granite

Figure 6 shows compressional and shear ultrasonic velocity data for Westerly granite (Coyner, 1984) and a comparison between Biot, Gassmann, and our prediction for saturated velocity. The pressure dependent porosity is shown in Figure 7. At high stress the Biot prediction is in good agreement with the saturated compressional velocity data. At low stress the saturated compressional velocity data exceed the Biot predictions by as much as 5 percent. In this case, the Biot and Gassmann predictions are essentially the same due to the low porosity, $\phi \approx .8$ percent, of Westerly granite. Our model is identical to Biot's model at the highest stress (100 MPa) where porosity is dominated by stiff pores of comparable compressibility. At low stress, a distribution of pore compressibilities due to the presence of both soft and stiff porosity leads to unrelaxed pore pressure gradients within the pore space and hence our unrelaxed velocity predictions are higher than the Biot predictions. Our model is within 1 percent agreement with the compressional velocity over the full range of stress from .3 to 100 MPa. For shear velocity, our model predicts higher velocities than Biot and Gassmann predictions at low stress, and is within 3 percent agreement of shear velocity over the full range of stress.

Tight gas sandstone

Figure 8 shows ultrasonic compressional and shear velocity data and a comparison between Biot, Gassmann, and our prediction for saturated velocity in a tight gas sandstone from the Travis Peak Formation. The associated porosity is in Figure 9. Similar behavior to Westerly granite is observed for both compressional and shear velocity data against the various model predictions. For compressional and shear velocity, saturated data are within 2 percent of our model predictions.

Navajo sandstone

Figure 10 shows ultrasonic compressional and shear velocity data for Navajo sandstone (Coyner, 1984) with Biot, Gassmann, and our model predictions. The porosity data are shown in Figure 11. Because of higher porosity in Navajo sandstone, $\phi \approx 11.8$ percent, the difference between Biot and Gassmann predictions can be resolved. Again, Biot is within 1 percent agreement of compressional velocity at high stress. At low stress, Biot and Gassmann underestimate the data by as much as 5 percent. In contrast, our prediction is in mostly good agreement except for stresses lower than 20

Table 1. Sample properties

Rock Sample	Porosity (%)	Grain density (g/cm^3)	Mineral bulk modulus (GPa)
Westerly granite	.8	2.64	56
Tight gas sandstone	8.0	2.63	38
Navajo sandstone	11.8	2.63	36
Fontainebleau sandstone	16.0	2.65	38

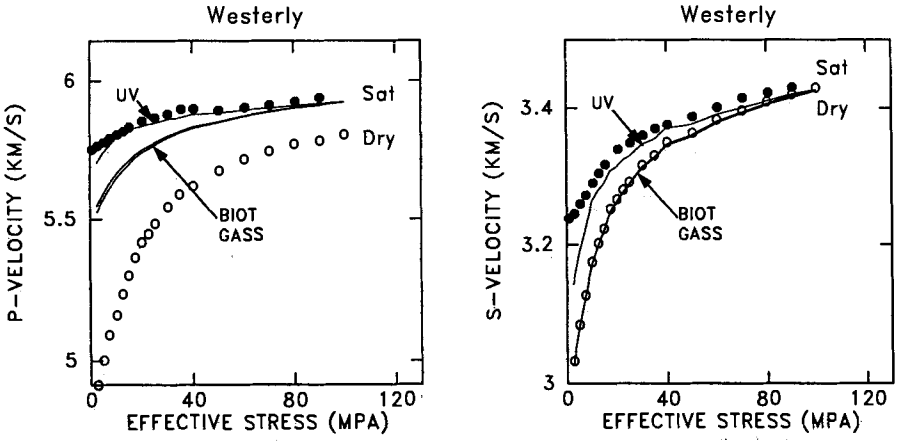

FIG. 6. Dry and fully water-saturated P and S velocities as a function of effective stress in Westerly granite (Coyner, 1984). Good agreement between the data and our high-frequency prediction (uv) suggests that pore fluids at lab frequency (.8-.9 MHz) are unrelaxed.

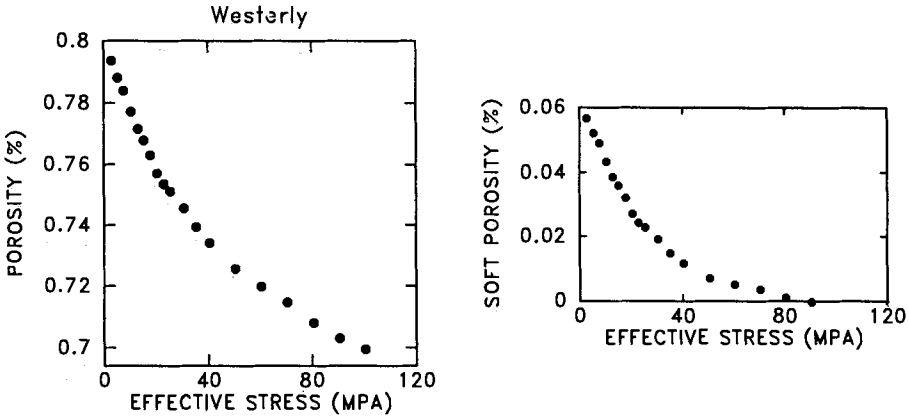

FIG. 7. Porosity versus effective stress in Westerly granite (Coyner, 1984). Soft porosity calculated from total porosity versus stress data is used in model predictions for unrelaxed P and S velocities.

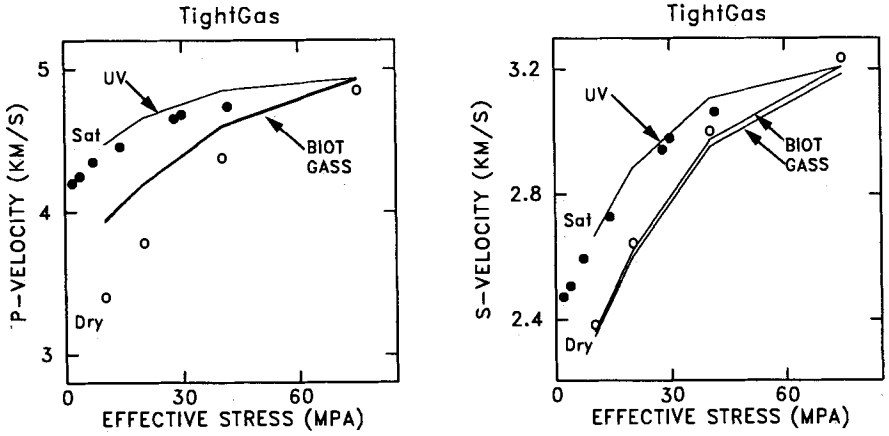

FIG. 8. Dry and brine saturated P and S velocities as a function of effective stress in a tight gas sandstone. Good agreement between the data and our high frequency prediction suggests that pore fluids at lab frequency (1 MHz) are unrelaxed.

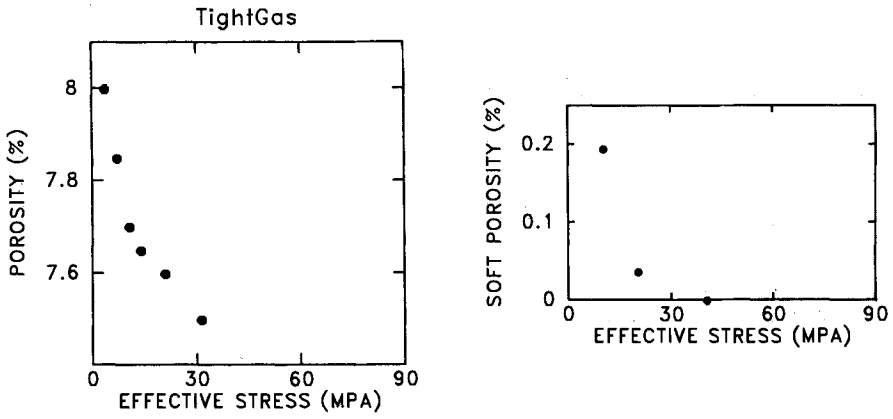

FIG. 9. Porosity versus effective stress in a tight gas sandstone. Soft porosity calculated from total porosity versus stress data is used in model predictions for unrelaxed P and S velocities.

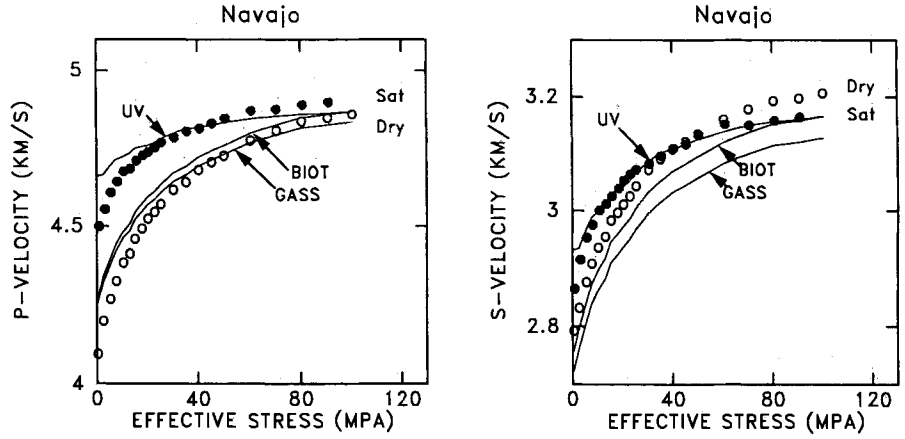

FIG. 10. Dry and water-saturated P and S velocities as a function of effective stress in Navajo sandstone (Coyner, 1984). Good agreement between the data and our high-frequency prediction suggests that pore fluids at lab frequency (.8-.9 MHz) are unrelaxed.

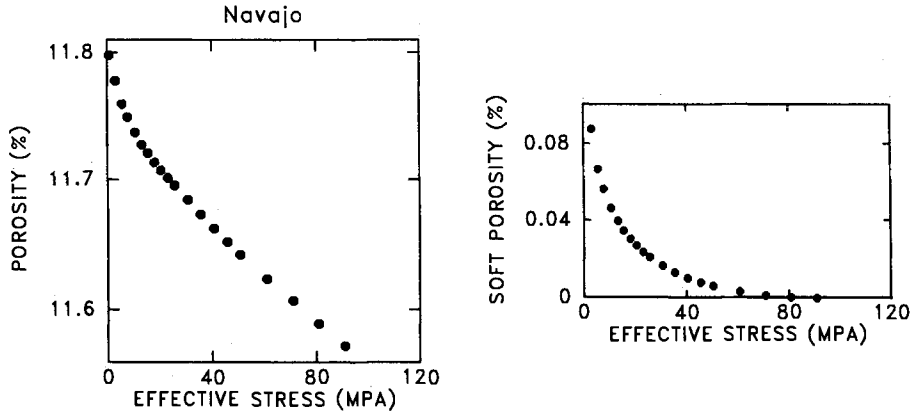

FIG. 11. Porosity versus effective stress in Navajo sandstone (Coyner, 1984). Soft porosity calculated from total porosity versus stress data is used in model predictions for unrelaxed P and S velocities.

MPa where it overestimates the saturated data by 3 percent. (An overestimation is acceptable since our model attempts to estimate the high-frequency limit or upper bound to the unrelaxed velocities.) Similarly, our model predictions for shear velocity are in much better agreement with the saturated data than the Biot and Gassmann predictions.

Fontainebleau sandstone

Figure 12 shows ultrasonic compressional and shear velocity data for Fontainebleau sandstone (Han, 1986) with Biot, Gassmann, and our model predictions for saturated velocity. The porosity versus stress data are shown in Figure 13. Overall agreement of our model is good, within 2 percent, for both compressional and shear velocity. We note, however, that in the case of Fontainebleau, our predictions underestimate the data at the highest pressure (50 MPa). One explanation is the following. We assume in our work that non-Biot dispersion disappears at sufficiently high pressure, and we associate this with the reduction of soft porosity. We use this to equate the stiff pore compressibility ($d\phi/d\sigma$) in equation (8) with the measured high-pressure compressibility. Our model will underestimate the velocity whenever the highest pressure data still has non-Biot dispersion and/or substantial unclosed soft porosity.

CONCLUSIONS

The important result of equation (10) is that to first order the magnitude of the grain scale dispersion can be estimated simply from the measured decrease of the dry rock compressibility with pressure. A second order correction is proportional to the measured change of porosity with pressure. Higher order corrections require more details of the distribution of the soft porosity. In our data examples we found that the second order and higher porosity-related corrections had essentially no change on the result. This is fortunate since (1) porosity versus pressure data are less often available than compressibility versus pressure and (2) estimates of the porosity-related terms require more and more assumptions about the pore space geometry, which we have tried to avoid. A simple interpretation of equation (10) is that at any pressure, filling all of the thin compliant pores with viscously unrelaxed fluid is, to first order, mechanically the same as compressing them closed or filling them with mineral. The second order correction recognizes that this is an

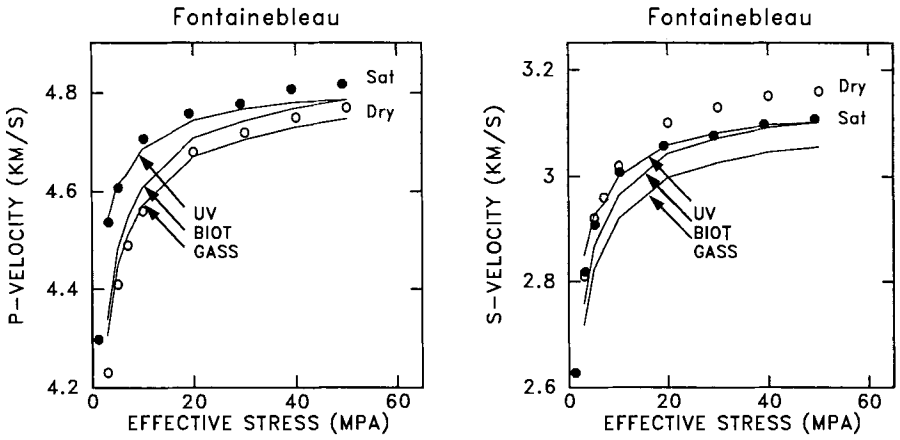

FIG. 12. Dry and water-saturated P and S velocities as a function of effective stress in Fontainebleau (Han, 1986). Good agreement between the data and our high frequency prediction suggests that pore fluids at lab frequency (.8-.9 MHz) are unrelaxed.

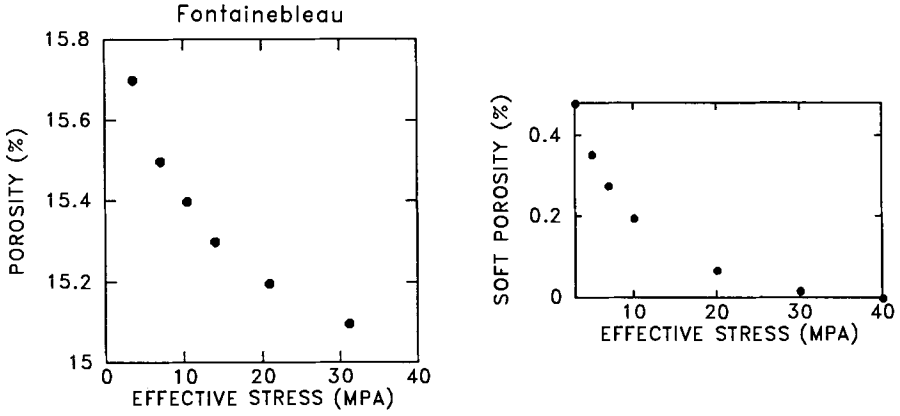

FIG. 13. Porosity versus effective stress in Fontainebleau (Han, 1986). Soft porosity calculated from total porosity versus stress data is used in model predictions for unrelaxed P and S velocities.

overestimate proportional to the difference of fluid and mineral compressibilities, times the volume of the soft porosity.

The second important result, equation (22), is that local flow effects in shear are proportional to those in bulk. This simply illustrates that the effects are both related to compression of soft porosity.

The key assumptions of our model are the following:

(1) As with Gassmann's (1951) model, the mineral matrix is assumed to be elastically homogeneous and isotropic. The effects of pore distribution and dramatically contrasting grains such as soft clays are still under study.

(2) The viscously unrelaxed parts of the pore space are assumed to be essentially the same parts of the pore space that are reduced or eliminated under high confining stress. This is most easy to visualize with conventional ideal crack models, but we feel it applies also to virtually any "crack like" feature such as arbitrarily irregular microcracks, grain contacts, and narrow tips of otherwise fat pores.

(3) A corollary to assumption (2) is that the compressibility of stiff pore fractions at any pressure is the same as the total pore compressibility at high pressure.

(4) Another corollary to assumption (2) is that the volume of the soft porosity at any pressure can be estimated as the difference between the total porosity and the extrapolation of the high pressure porosity versus pressure trend (see Figure 14). This implies that the two fractions of the pore space are somehow separate; that stiff pores stay stiff and soft pores stay soft until they close under compression. Although this might not be strictly true, the fact is that the soft porosity correction is very slight and improvements in it appear to be of little consequence.

We feel that our assumptions are justified by (1) the generally good agreement of the model and data, (2) the predicted strong relation between shear and bulk properties which is supported by the excellent agreement with shear velocities in particular, and (3) the fact that the formulation, equations (10) and (22), is entirely in terms of measurable bulk properties only, without the need for poorly determined parameters such as aspect ratios.

As illustrated by the Fontainebleau sandstone example, (Figure 12), the method performs most poorly when there is non-Biot or local flow dispersion at high pressure. This apparently is a violation of assumption (3). One possibility is that the model is not appropriate for those rocks; another possibility is that the model would perform better if higher pressure data were available, such that more of the soft porosity is compressed.

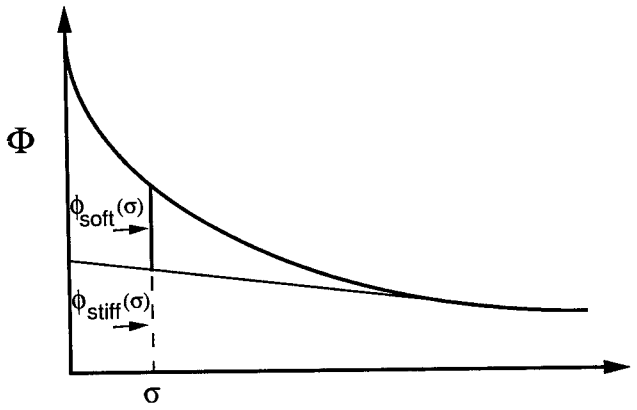

FIG. 14. Schematic plot of dry rock porosity versus pressure. The volume of the soft porosity at any pressure is estimated as the difference between the total porosity and the extrapolation of the high-pressure trend.

ACKNOWLEDGMENTS

This work was supported by the Stanford Rock Physics and Borehole project and Gas Research Institute contract 5087-260-1635. The authors thank Amos Nur and Ken Winkler for useful discussions, and Mike Batzle, Robert Haupt, Bill Dillon, and the GEOPHYSICS Associate Editor for careful and constructive reviews of the manuscript.

REFERENCES

Biot, M. A., 1956a, Theory of propagation of elastic waves in a fluid saturated porous solid. I. Low-frequency range: J. Acoust. Soc. Amer., **28**, 168–178.

——— 1956b, Theory of propagation of elastic waves in a fluid-saturated porous solid. II. Higher-frequency range: J. Acoust. Soc. Amer., **28**, 179–191.

——— 1962a, Generalized theory of acoustic propagation in porous dissipative media: J. Acoust. Soc. Amer., **34**, 1254–1264.

——— 1962b, Mechanics of deformation and acoustic propagation in porous media: J. Appl. Physics, **33**, 1482–1498.

Carmichael, R. S., 1981, Handbook of physical properties of rocks: C.R.C. press.

Coyner, K. B., 1984, Effects of stress, pore pressure, and pore fluids on bulk strain, velocity, and permeability in rocks: Ph.D. thesis, Massachusetts Inst. Tech.

Coyner, K. B., and Cheng, C. H., 1985, New laboratory measurements of seismic velocities in porous rocks: Geophysics, **50**, 309.

Gassmann, F., 1951, Uber die elastizitat poroser medien: Vier. der Natur Gesellschaft, **96**, 1–23.

Han, D., 1986, Effects of porosity and clay content on acoustic properties of sandstones and unconsolidated sediments: Ph.D. thesis, Stanford University.

Jaeger, J. C., and Cook, N. G. W., 1969, Fundamentals of rock mechanics: Chapman and Hall.

Keller, J. D., 1989, Acoustic wave propagation in composite fluid saturated media: Geophysics, **54**, 1554–1563.

Mavko, G., and Nur, A., 1979, Wave attenuation in partially saturated rocks: Geophysics, **44**, 161–178.

Murphy, W. F., Winkler, K. W., and Kleinberg, 1984, Contact microphysics and viscous relaxation in sandstones, *in* Johnson, D. L., and Sen, P. N., Eds., Physics and Chemistry of Porous media: Am. Inst. Phys.

O'Connell, R., and Budiansky, B., 1974, Seismic velocities in dry and saturated cracked solids: J. Geophys. Res., **79**, 5412–5426.

——— 1977, Viscoelastic properties of fluid-saturated cracked solids: J. Geophys. Res., **82**, 5719–5736.

Stoll, R. D., and Bryan, G. M., 1970, Wave attenuation in saturated sediments: J. Acoust. Soc. Am., **47**, 1440–1447.

Walsh, J., 1965, The effect of cracks on the compressibility of rock: J. Geophys. Res., **70**, 381–389.

Wang, Z., and Nur, A., 1988, Velocity dispersion and the "local flow" mechanism in rocks: 58th Ann. Internat. Mtg., Soc. Explor. Geophys., Expanded Abstracts, 928–930.

Winkler, K., 1985, Dispersion analysis of velocity and attenuation in Berea sandstone: J. Geophys. Res., **90**, 6793–6800.

——— 1986, Estimates of velocity dispersion between seismic and ultrasonic frequencies: Geophysics, **51**, 183–189.